BNL-225553-2024-JAAM

GRP-COEE-33

Evolution and Interplay of Lithium Metal Interphase Components Revealed by Experimental and Theoretical Studies

S. Tan

To be published in "Journal of the American Chemical Society"

April 2024

Chemistry Department

Brookhaven National Laboratory

U.S. Department of Energy

USDOE Office of Energy Efficiency and Renewable Energy (EERE), Office of Sustainable Transportation. Vehicle Technologies Office (VTO)

DISCLAIMER

Evolution and interplay of lithium metal interphase components revealed by experimental and theoretical studies

Sha Tan[1,‡], Dacheng Kuai[2,‡], Zhiao Yu[3], Saul Perez-Beltran[2], Muhammad Mominur Rahman[1], Kangxuan Xia[1], Nan Wang[1], Yuelang Chen[3], Xiao-Qing Yang[1], Jie Xiao[4], Jun Liu[4], Yi Cui[5,6], Zhenan Bao[3], Perla B. Balbuena[2,*], Enyuan Hu[1,*]

[1] Chemistry Division, Brookhaven National Laboratory, Upton, NY, USA 11973

[2] Department of Chemical Engineering, Texas A&M University, College Station, TX, USA 77843

[3] Department of Chemical Engineering, Stanford University, Stanford, CA, USA 94305

[4] Energy and Environment Directorate, Pacific Northwest National Laboratory, Richland, WA, USA 99352

[5] Department of Materials Science and Engineering, Stanford University, Stanford, CA, USA 94305

[6] Stanford Institute for Materials and Energy Sciences, SLAC National Accelerator Laboratory, Menlo Park, CA 94025

ABSTRACT: Lithium metal batteries (LMB) have high energy densities and are crucial for clean energy solutions. The characterization of lithium metal interphase is fundamentally and practically important but technically challenging. Taking advantage of synchrotron x-ray which has the unique capability of analyzing crystalline/amorphous phases quantitatively with statistical significance, we study the composition and dynamics of LMB interphase for a newly developed important LMB electrolyte that is based on fluorinated ether. Pair distribution function analysis revealed the sequential role of anion and solvent in interphase formation during cycling. The relative ratio between Li_2O and LiF first increases and then decreases during cycling, suggesting suppressed Li_2O formation in both initial and long extended cycles. Theoretical studies revealed that in initial cycles, this is due to the energy barrier in many-electron transfer. In long extended cycles, the anion decomposition product Li_2O encourages solvent decomposition by facilitating solvent adsorption on Li_2O which is followed by concurrent depletion of both. This work highlights the important role of Li_2O in transitioning from anion-derived interphase to a solvent-derived one.

INTRODUCTION

To address the clean energy imperative, it is crucial to electrify our energy consumption, particularly in the transportation sector. Among potential energy storage solutions, lithium metal batteries (LMBs) are prominent due to their superior energy density, which arises from the utilization of lithium metal as the anode and nickel-rich transition metal oxide as the cathode.[1] As the electrolyte is usually not thermodynamically stable against the electrode, an interphase resulting from the decomposition of electrolyte is formed between the electrolyte and the electrode.[2] For LMB to have an extended cycle life, stabilization of the interphase between electrodes and the electrolyte is critical.[3, 4] The solid-electrolyte-interphase (SEI) on the lithium metal anode (LMA) is of particular significance.[5] Therefore, an in-depth understanding of SEI is essential to electrolyte design and interphase engineering. However, characterizing SEI is very demanding for several reasons.[6, 7] SEI typically comprises light-element compounds with both crystalline and amorphous constituents and is extremely sensitive to air and radiation exposure. In this study, we take an integrative approach, combining experimental and theoretical efforts, to study lithium metal SEI in great depths. As demonstrated in our previous research[8, 9], synchrotron-based high flux x-ray total scattering has several advantages in characterizing SEI, such as minimal beam damage, capability to characterize both crystalline and amorphous components, high reproducibility across cells, and significant statistical relevance. In addition to instrumental characterization, theoretical simulation approaches offer rich information of the fundamental chemical processes that account for the SEI structures and properties.[10] From the first principles, the interfacial electrochemistry can be resolved at atomic level, enabling the identification of plausible SEI components. The experiment and simulation methods complement each other and bring a cross-validated picture for the complex SEI system.

Among the various electrolyte systems developed for LMB, two demonstrate exceptional potential, facilitating stable cycling of LMB in ampere-hour (Ah) scale pouch cells under practical conditions. The first is the high concentration electrolyte (HCE) using lithium salt (such as lithium bis(fluorosulfonyl) imide, also known as LiFSI) dissolved in a strong solvating solvent such as 1,2-dimethoxyethane[11]. Such composition leads to a unique solvation structure that facilitates an anion-derived interphase which has been shown to be more robust and stable than the solvent-derived interphase typical of low concentration electrolyte. For further optimization, diluents such as 1,1,2,2-tetrafluoroethyl-2,2,3,3-tetrafluoropropyl ether are incorporated, forming localized high concentration electrolyte (LHCE), to effectively mitigate electrolyte viscosity,

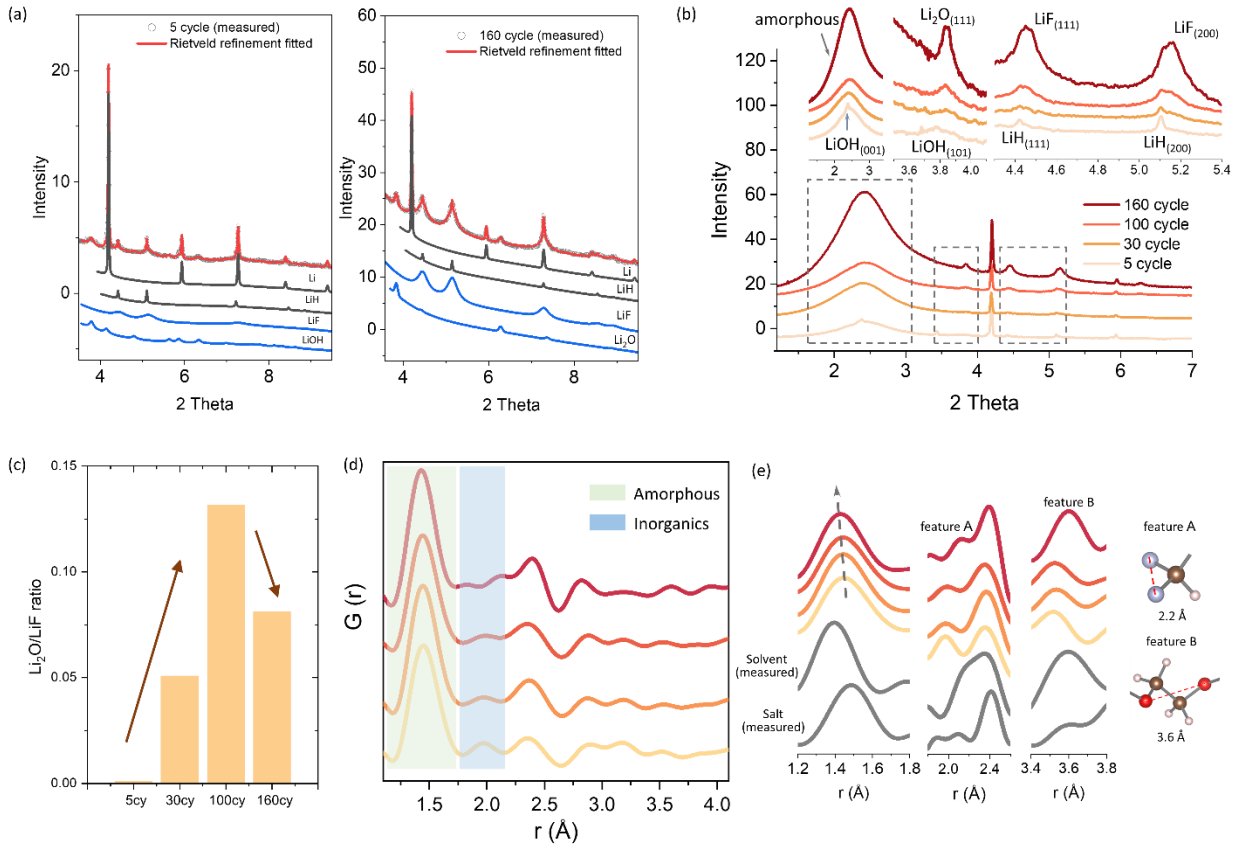

Figure 1. XRD and PDF of SEI from various cycles. (a) Rietveld refinement of XRD data for SEI from the 5th (left) and 160th (right) cycles. (b) XRD of SEI with regions of interest magnified in the inset graph. (c) The Li_2O/LiF relative ratio during cycles. (d) PDF patterns of SEI. The green and the blue peak correspond to amorphous and inorganic components respectively. (e) In-depth analysis of the PDF data together with reference patterns for both the F5DEE solvent and the LiFSI salt.

improving both wettability and transport properties.[12, 13] The second notable system is the single-solvent electrolyte based on fluorinated ether. A typical example is 1.2M LiFSI dissolved 1-(2,2-difluoroethoxy)-2-(2,2,2-trifluoroethoxy)ethane (F5DEE), developed by Stanford's group[14], whose working mechanism and interphase are still little understood.

Here we employ synchrotron-based scattering and spectroscopy techniques to investigate the SEI resulting from the F5DEE electrolyte. Using Rietveld refinement of X-ray diffraction (XRD) coupled with pair distribution function (PDF) analysis, we achieved a quantitative assessment of the crystalline components and a qualitative evaluation of the amorphous components within the SEI. The utilization of X-ray absorption spectroscopy (XAS) at both total electron yield (TEY) and partial fluorescence yield (PFY) allows compositional investigation at different probing depths. By analyzing the SEI across various cycles, we delineated its evolutionary trajectory. Coupling with the theoretical calculations, the decomposition mechanism of the F5DEE electrolyte has been thoroughly investigated. High consistency was observed between our experimental findings and theoretical calculations. Collectively, these results unveil a previously unidentified mechanism for both crystalline and amorphous phases within SEI. The mutual interactions and dynamics among these components play a pivotal role in determining eventual SEI composition.

RESULTS AND DISCUSSION

The synchrotron XRD results for the lithium metal SEI derived from the F5DEE electrolyte (full cell electrochemistry shown in Figure S1) are presented in Figures 1a and 1b. The very broad bump at 2.5° is attributed to the amorphous components from electrolyte decomposition and its intensity steadily grows with continued cycling. The sharp peaks in the SEI XRD data can be fitted well using Rietveld refinement (Figure 1a, Figure S2, S3). Contributions from each phase to the XRD data are also presented, clarifying the origin of each individual peak. With the XRD data fully analyzed, we discuss in detail the evolution of the crystalline components as illustrated in Figure 1b.

During the initial cycles, LiOH is present in the SEI owing to the native surface film on the LMA and the side reaction with the water contamination in the electrolyte. After 30 cycles, the conversion of LiOH to Li_2O on the LMA is observed as discussed in our previous work[9]. With the increasing cycle number, further reduction of FSI anion is observed, producing more and more LiF and Li_2O, which are believed to be beneficial components for achieving lithium metal protection. Using the Rietveld refinement, quantitative analysis of the relative Li_2O/LiF amount during cycling is summarized in Figure 1c. The Li_2O/LiF ratio starts with very low values and reaches the maximum after 100 cycles followed by a gradual decrease, indicating the

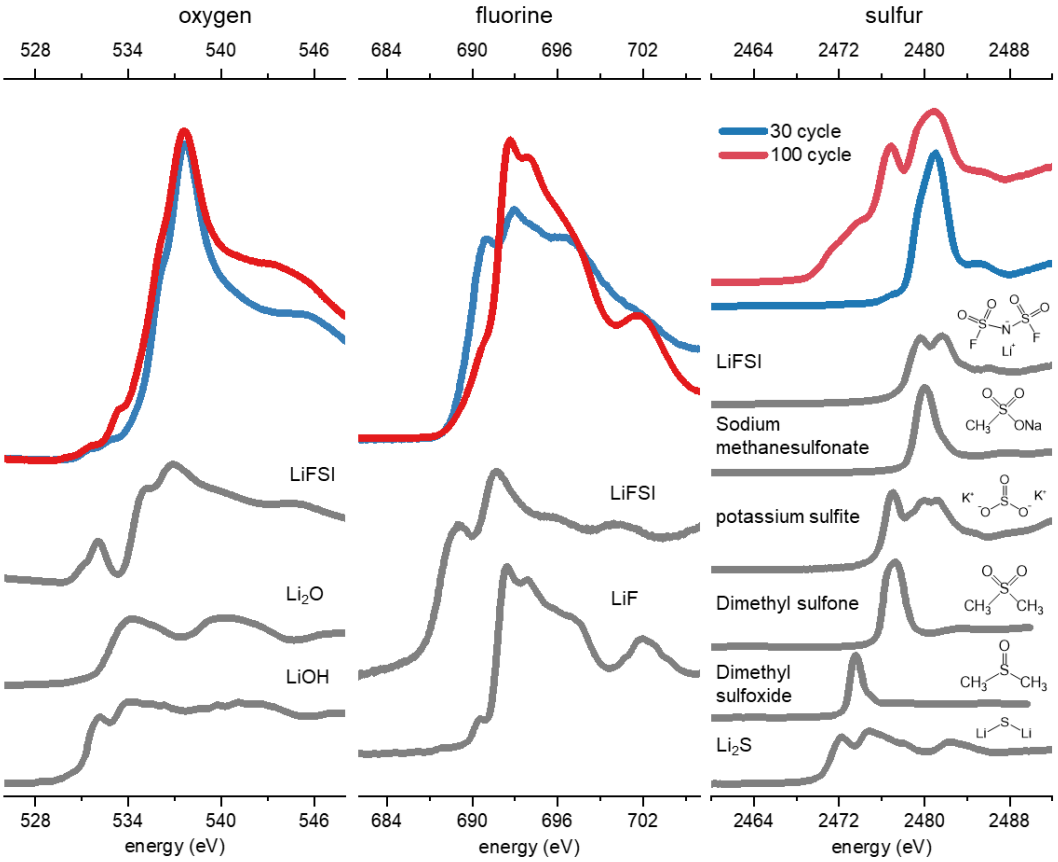

Figure 2. Oxygen, fluorine and sulfur XAS of SEI from different cycles. Reference spectra are also shown.

suppressed formation of Li_2O in both the initial cycles and the extended cycles. In contrast, LiF amount has steady increase during cycling.

PDF is a total scattering technique utilizing signals from both Bragg scattering and diffuse scattering. Therefore, it can reveal information regarding both crystalline and amorphous components (Figure 1d). As shown in our previous work,[8] the first PDF peak at around 1.5 Å is uniquely attributable to amorphous components which contain short bonds such as carbon-based C-O/F/H bonds and sulfur-based S-N/F/O bonds. The intensity of this peak serves as a convenient indicator of the abundance of amorphous components in the SEI. The peak around 2.0 Å corresponds to lithium-based Li-O/F bonds which are mostly found in inorganic crystalline species and therefore its intensity provides insight into the abundance of inorganics species in the SEI. Comparing the intensities of the 1.5 Å and 2.0 Å peaks indicates that the SEI consistently has a high content of amorphous components, which becomes even more pronounced after extended cycles.

Both XRD and PDF confirm the high content of amorphous species in the SEI. To understand the origin of the amorphous components in the SEIs, particularly whether they arise from anions or solvents, a more in-depth analysis of the first PDF peak at 1.5 Å is performed (Figure 1e). The bond lengths of sulfur-based bonds are slightly longer than those of carbon-based bonds, a fact also reflected in the PDF data of both LiFSI salt and the F5DEE solvent. In the PDF data of initial SEI, the 1.5Å peak largely aligns with the first PDF peak of the LiFSI salt, suggesting that the initial amorphous species is primarily from anion decomposition. As the cycling progresses, the initial peak in the PDF shifts to a lower *r* value, indicating an increasing involvement of solvents in the SEI formation. This point is supported by distinct features around 2.2 Å and 3.6 Å. The PDF data of F5DEE solvent indicates that these features arise from indirect correlations between fluorine atoms (feature A) and oxygen atoms (feature B). Importantly, these characteristics are not displayed by FSI anions, and the corresponding peaks are absent in the FSI PDF data, which suggests their capabilities of pinpointing the presence of solvent-derived species.

Oxygen and fluorine XAS (in TEY mode) were measured to obtain more insights about SEI composition and its evolution. As confirmed by XRD (Figure S4) results, there is no crystalline LiFSI residue on the cycled Li anode. The oxygen, fluorine and sulfur signals mainly originate from FSI decomposition products. Compared to the pristine LMA (Figure S5), the oxygen XAS peak shape changes after cycling, indicating the electrolyte-derived oxygen-containing species formation in the SEI. At the 30th cycle, oxygen TEY XAS (Figure 2) in general resembles that of the LiFSI salt XAS spectrum, with a notable exception being the 531.5 eV peak, is probably attributed to the decomposition of FSI

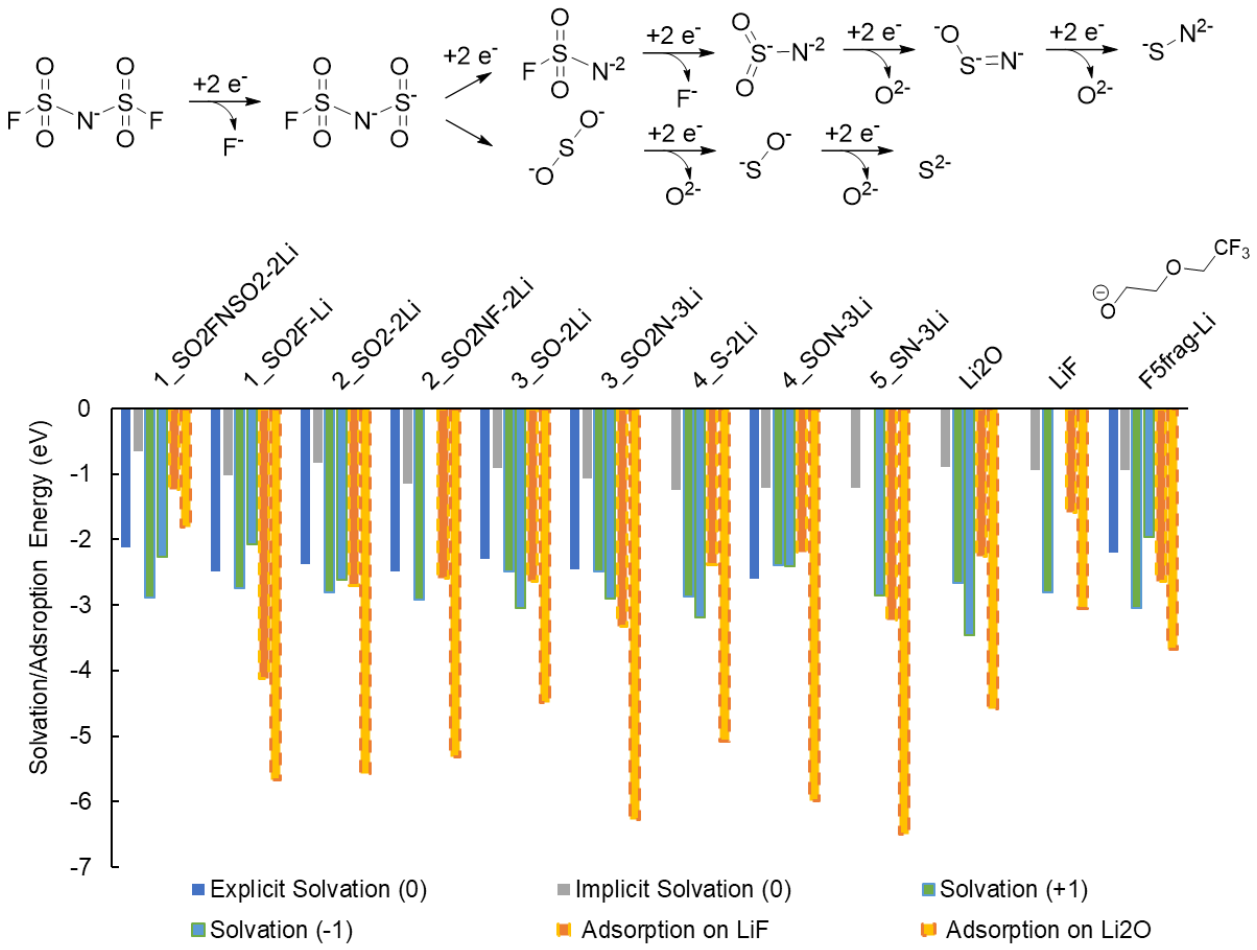

Figure 3. Solvation and adsorption energetics of LiFSI and F5DEE decomposition fragments (see SI for calculation details).

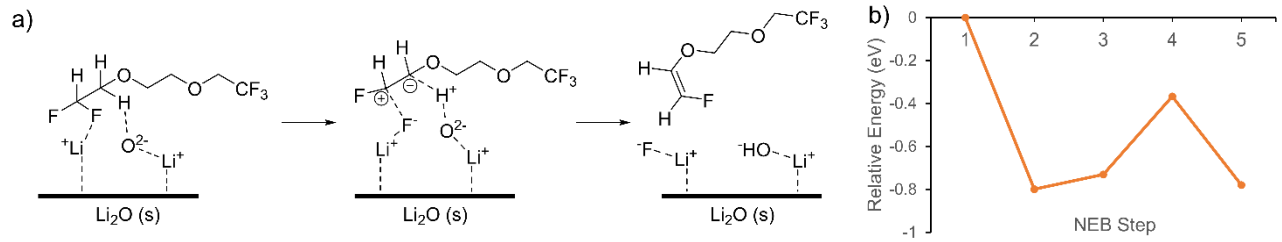

Figure 4. F5DEE defluorination on Li_2O surface (a) mechanism and (b) energy profile analyzed based on NEB calculations.

during which S-N/O bonds cleavage, redistributing the electrons and eliminating XAS peaks corresponding to the original bonds. The TEY XAS data at this stage indicates a minimal presence of Li_2O in the top surface of SEI. After 100 cycles, a distinct peak emerges around 533 eV in the oxygen TEY XAS spectrum, which is indicative of Li_2O formation.[15] This observation aligns well with earlier XRD findings. Besides the Li_2O, the notable peak at 537eV after 30 and 100 cycles suggests the presence of large amount of FSI-derived oxygen-containing amorphous species.

In the fluorine K-edge results (Figure 2), the most pronounced peak for LiF situates at approximately 692.5 eV, while for LiFSI, it's around 691 eV. This variation serves as a qualitative measure to determine the relative abundance of LiF and FSI-derived amorphous entities. At the 30th cycle, fluorine TEY XAS has very strong peak at around 691 eV, indicating FSI-derived amorphous components in large quantities. At the 100th cycle, fluorine TEY XAS changes significantly, with the 692.5 eV peak becoming dominant and the overall spectrum is almost the same as that of the LiF reference spectrum, suggesting further LiF accumulation owing to the further FSI anion reduction during the electrochemical cycling. XAS measurement in PFY mode was also performed, offering insights more representative of the bulk SEI compared to the TEY mode. The result is shown in Figure S6, suggesting there are a large amount of FSI-derived species in the SEI, in agreement with the XRD/PDF results.

Sulfur K-edge XAS result describes the salt/anion decomposition products in the SEI. The results were measured at PFY mode, its peak intensity represents the chemical species concentration within the interphase. In Figure 2, the higher peak intensity after 100-cycle suggests the anion decomposition products accumulation. After FSI decomposition, changes of sulfur coordination environment result in distinct changes in sulfur XAS peak shape and position,

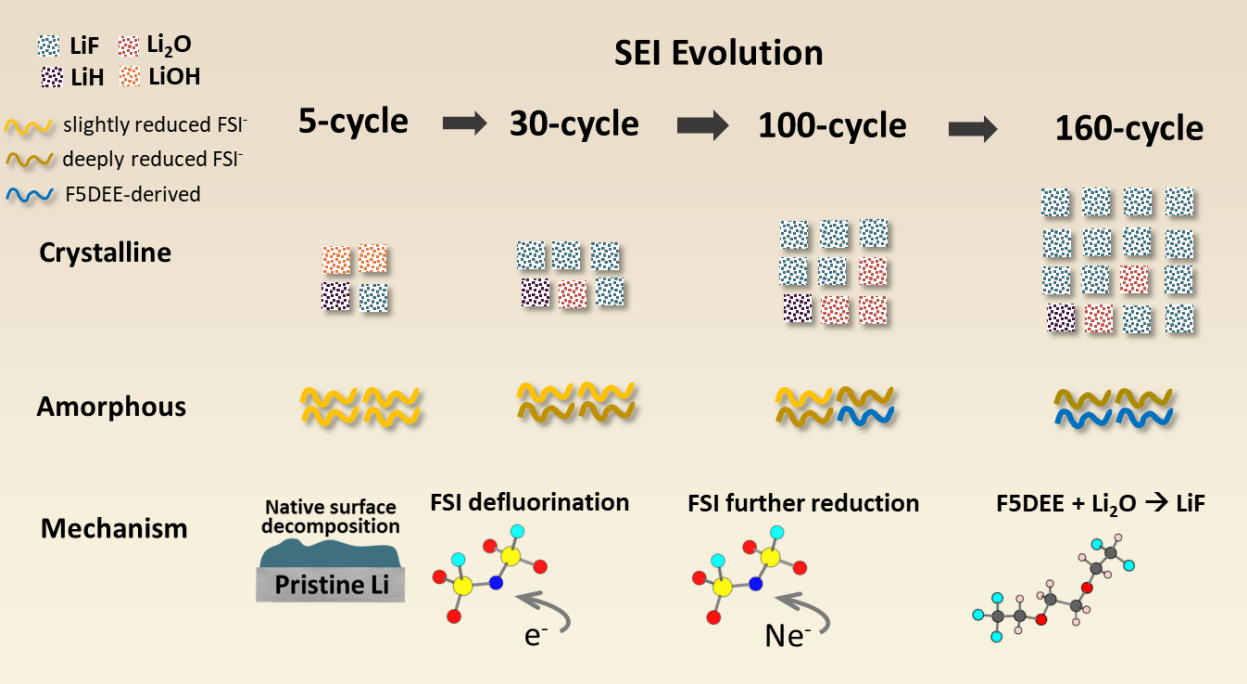

Figure 5. Illustration of the SEI evolution in F5DEE electrolyte. The primary findings from both the experimental observations and calculations are presented, revealing notable consistency between the two.

differing from those observed with LiFSI salt. Furthermore, the sulfur species in the interphase kept evolving during the electrochemical cycling, as suggested by the peak growth at the lower energy region (below 2480 eV). Specifically, sulfonyl species dominate after 30 cycles, while more reduced sulfur components, such as trace amount of Li_2S emerge after 100 cycles, suggesting the further reduction of FSI^- on the anode surface.[16]

To elucidate SEI formation from F5DEE electrolyte decomposition, atomistic models were used to investigate interfacial electrochemistry. Ab initio molecular dynamics (AIMD) simulations showed spontaneous dissociation of F5DEE and LiFSI on Li(100) surfaces, with electronegative atoms (O and F) coordinating with Li^+. Bader charge analysis revealed continuous electron transfer from Li metal to lithiated F5DEE and LiFSI without high-spin state intermediates. We term these events "lithium-ion-coupled electron transfer" (LICET).

F5DEE reacts with Li metal without external potential, altering its electronic structure upon reduction, with spin density mainly on the CHF_2-side (Figure S7), leading to a high priority of defluorination and C-O cleavage on the same side of the structure. Within the time scale probed in AIMD, F5DEE transforms into the LiF, negatively charged $C_2H_3^-$ and $CF_3CH_2OCH_2CH_2O^-$ structures. This reaction between Li and F5DEE is also confirmed by X-ray photoelectron spectroscopy (XPS) results (Figure S8), generating LiF and C-F species after soaking Li foil in F5DEE. The dielectric constant (ε) of pure F5DEE was measured to be 11.02. Considering that the dielectric constant is negatively correlated with the salt concentration in practical electrolyte systems,[17] we computed the LICET free energy profiles at ε = 4.24 and 10.13 as Figure S9 demonstrates. The energy surfaces show similar patterns in these two conditions, and each step is only controlled by electron transfer without outstanding energy barriers.

Different solvation shells form via Li-O/F coordination in F5DEE and LiFSI. The Li-O semi-covalent bonding is significantly more stable than Li-F coordination. F5DEE can easily form chelating bonds with Li^+ either singly or dually in joint with FSI^- (Figure S10a). Meanwhile, the joint chelation among F5DEE, Li^+ and FSI^- is prominently stronger than that in FSI- or F5DEE- only cases. This suggests that the solvation shell in liquid electrolyte should be primarily composed of FSI-Li-F5DEE clusters (contact ion pairs). In the meantime, FSI^- bond cleavage priorities during the reduction-induced fragmentation are found to be dependent on the solvation structure. Defluorination (S-F cleavage) has higher thermodynamic priority than N-S cleavage without solvent engagement, while the opposite scenario takes place when Li^+ is coordinated with F5DEE (see Figure S10b for details). The intermediates and pathways after the S-N/F breaking steps are highly overlapped. Comparing the free energy profiles of F5DEE and LiFSI (Figure S11), each step of the LICET-induced dissociation of LiFSI is more thermodynamically favorable than F5DEE, meaning LiFSI has higher decomposition kinetics in competitive conditions. This also agrees well with the experimental finding that the LiFSI degradation product was identified in the initial cycles due to fast salt decomposition, and the increase of F5DEE fragment signals in longer runs due to the higher population abundance in electrolyte and gradual dissociation kinetics.

AIMD revealed coexisting pathways led by N-S breaking and S-F breaking in LiFSI degradation, which agrees with the even and symmetric distribution of high-spin electronic density in the reduced $LiFSI^-$ structure. Here we analyzed the FSI^- degradation based on the AIMD trajectories at the B3LYP/aug-cc-pVDZ level of theory. In contrast to the $LiPF_6$ case,[18] the LiFSI decomposition is less favorable in higher dielectric environment as Figure S11 indicates. Similar to F5DEE, all LICET steps in LiFSI dissociation are

highly spontaneous. Within the 1 ps of AIMD simulation, FSI^- fully decompose into single-atomic fragments including O^{2-}, S^{2-}, F^-, and the only fragment that maintains internal chemical bonding is $[S\text{-}N]^{3-}$ which was detected together with Li_3N signals in the XPS of SEI[19]. In addition, Camacho-Forero et al captured the N^{3-} formation from AIMD with a longer simulation time length[20]. According to the N-S bond scan in $Li_3[NS]$ and $Li_5[NS]$ clusters (Figure S12), while the last LICET step of FSI^- degradation in generating Li_3N and Li_2S is thermodynamically favorable, the kinetics are still primarily controlled by the reductive Li availability. This may explain why only trace amount of Li_2S and little if any Li_3N are detected in the experimental results (Figure S13). Li_2CO_3, a common component of the SEI in carbonate electrolyte, was not detected in the SEI of F5DEE. The first-principle simulations also found no evidence associated with carbonate formation pathway. This may not be surprising as the formation of Li_2CO_3 requires oxidation of ethereal C-O bond, a reaction that is challenging to achieve in the reducing environment present at a lithium metal anode.

Both F5DEE and LiFSI initially produce LiF as a major degradation product in early interfacial degradation stages. Full LiFSI degradation yields more Li_2O than LiF. Understanding the fragment preferences for adsorption versus dissolution is vital to speculate the SEI composition. Here we compared solvation and adsorption energetics of the LiFSI and F5DEE degradation fragments (Figure 3). In general, especially for short-length fragments, explicit solvent-fragment interactions make solvation more competitive than adsorbing to the LiF crystalline surface. The fragment adsorption on Li_2O is predominantly more favorable than all other dissolution and adsorption events, including the Li_2O growth (Li_2O adsorption to Li_2O surface). The major F5DEE fragmentation species also has such adsorption and solvation patterns, suggesting the potential organic components in SEI. Based on the prominent favorability of adsorption on Li_2O, an amorphous SEI morphology with stacked Li_2O-fragment-Li_2O structures is plausible. Further SEI structural elucidation could benefit from three-dimensional kinetic Monte Carlo simulations.

As discussed, fragment adsorption to Li_2O surface is more favorable than dissolution. However, AIMD simulation indicates that F5DEE molecule can easily react with Li_2O and fluorinate the SEI surface as Figure 4 and Figure S14 demonstrate. The Bader charge analysis confirms that such interfacial F5DEE-Li_2O reaction does not involve external charge flow.[21, 22] Nudged elastic band (NEB) theory calculations reveal a low energy barrier of 0.364 eV. In addition to yielding LiOH in SEI, this secondary SEI surface fluorination can lead to many consequences, including 1) elimination of Li_2O on SEI-electrolyte interface; 2) easy dissolution of LiFSI decomposition fragment and less diverse species distribution in SEI; 3) amorphous morphology of LiF-Li_2O-LiOH stacking in SEI.

To further analyze the transition from LiOH to Li_2O at LiOH-Li boundaries, as suggested from our previous work[9], we performed an AIMD simulation as depicted in Figure S15. No O-H cleavage occurred in the 107 ps simulation time at the LiOH-Li grain boundary, suggesting even more rigorous reaction requirements. According to the NEB calculations, despite that the overall thermodynamic favorability, the O-H cleavage requires an energy barrier of 5.41 eV on the Li(100) surface, and 5.30 eV on Li(110) surface (see Figure S16 for complete energy profiles). This suggests LiOH to Li_2O conversion is kinetically slow, in agreement with previous literature report.[23] The 4.4 V external potential during charging process facilitates overcoming such a high energy barrier under the cell working temperatures. The relatively slow convoluted conversion from LiOH to Li_2O and LiH is thus quantitively analyzed from the atomistic perspectives.

It should be noted that the amount of LiH also changes throughout battery cycling. Initially, LiH is primarily generated due to water contamination in the electrolyte and the presence of native LiOH on pristine Li foil. As battery cycling progresses, LiFSI decomposes first, leading to the formation of LiF and Li_2O, resulting in a decrease in the relative LiH amount. Further cycling leads to solvent decomposition and consequent LiH generation. The relative LiH percentage increases accordingly. In sum, the relative LiH content initially decreases and then increases, correlating with the sequence of solvent and salt decomposition.

CONCLUSIONS

In summary, we employed joint experimental and theoretical studies to reveal the SEI formation and evolution in F5DEE electrolyte. XRD offers quantitative insights into the crystalline inorganics present in the SEI, whereas PDF aids in distinguishing between amorphous solvent-derived organics and salt-derived inorganics. Furthermore, soft XAS enables the identification of chemical species, particularly amorphous components, and also provides information about trace SEI components. The integration of these techniques provides a comprehensive understanding of SEI composition. A schematic of the evolution of LMB SEI in F5DEE electrolyte is summarized and illustrated in Figure 5. Initially, the SEI is composed of native surface film, its derivatives and species resulting from anion decomposition. Salt defluorination promotes LiF formation. While the minor quantity of Li_2O could be attributed to the complex electron transfer process during anion reduction. The exclusive participation of anion decomposition in SEI formation also eliminates the possibility of forming reduced gaseous species such as ethylene at early stages of electrochemical cycling. After extended cycles, the SEI formed in previous cycles are further reduced, increasing Li_2O and LiF amount, and generating more reduced sulfur species. Theoretical calculations show that it is energetically favorable for F5DEE solvents to be adsorbed on Li_2O. The solvent and Li_2O further react to form LiF and solvent-derived molecular species. Such unique mechanism explains the observed dominance of LiF within the crystalline components of long-cycled SEI, while the amount of Li_2O remains relatively small. Meanwhile, it clarifies the evolution of amorphous components, that the amorphous phase initially dominated by FSI decomposition has increased solvent contributions during long-term cycling. Our joint experimental and computational studies reveal the dynamic relationship among SEI components and how that plays a pivotal role in guiding the evolutional trajectory of SEI. Notably, the synergistic alignment of experimental and theoretical insights offers unparalleled depth into the SEI for-

mation mechanism, a depth that would be elusive if pursued individually.

ASSOCIATED CONTENT

Supporting Information. Experimental and theoretical methods; electrochemical performance; XRD refinement results; decomposition pathways of solvent and salt; optimized structures. This material is available free of charge via the Internet at http://pubs.acs.org.

AUTHOR INFORMATION

Corresponding Author

* Email: balbuena@mail.che.tamu.edu (P.B.B.); enhu@bnl.gov (E.H.)

Author Contributions

‡ These authors contributed equally.

Notes

Authors declare that they have no competing interests.

ACKNOWLEDGMENT

The work done at Brookhaven National Laboratory was supported by the Assistant Secretary for Energy Efficiency and Renewable Energy, Vehicle Technology Office of the US Department of Energy (DOE) through the Advanced Battery Materials Research (BMR) Program, including Battery500 Consortium under contract no. DE-SC0012704. This research used beamlines 28-ID-2, 23-ID-2 and 8-BM of the National Synchrotron Light Source II, a US DOE Office of Science user facility operated for the DOE Office of Science by Brookhaven National Laboratory under contract no. DE-SC0012704. The cathode electrodes were provided by Cell Analysis, Modeling, and Prototyping (CAMP) Facility at Argonne National Laboratory. The CAMP Facility is fully supported by the DOE Vehicle Technologies Office. The computational studies were supported by the Assistant Secretary for Energy Efficiency and Renewable Energy, Office of Vehicle Technologies of the US Department of Energy through the Advanced Battery Materials Research (BMR) Program (Battery500 Consortium phase 2) under DOE contract No. DE-AC05-76RL01830 from the Pacific Northwest National Laboratory (PNNL). Computational resources from the Texas A&M University High Performance Research Computing are gratefully acknowledged.

REFERENCES

(1) Liu, J.; Bao, Z.; Cui, Y.; Dufek, E. J.; Goodenough, J. B.; Khalifah, P.; Li, Q.; Liaw, B. Y.; Liu, P.; Manthiram, A.; et al. Pathways for practical high-energy long-cycling lithium metal batteries. *Nat. Energy* **2019**, *4* (3), 180-186.

(2) Cao, X.; Jia, H.; Xu, W.; Zhang, J.-G. Review—Localized High-Concentration Electrolytes for Lithium Batteries. *J. Electrochem. Soc.* **2021**, *168* (1), 010522.

(3) Zhang, J.-G.; Xu, W.; Xiao, J.; Cao, X.; Liu, J. Lithium Metal Anodes with Nonaqueous Electrolytes. *Chem. Rev.* **2020**, *120* (24), 13312-13348.

(4) Wang, H.; Yu, Z.; Kong, X.; Kim, S. C.; Boyle, D. T.; Qin, J.; Bao, Z.; Cui, Y. Liquid electrolyte: The nexus of practical lithium metal batteries. *Joule* **2022**, *6* (3), 588-616.

(5) Tikekar, M. D.; Choudhury, S.; Tu, Z.; Archer, L. A. Design principles for electrolytes and interfaces for stable lithium-metal batteries. *Nat. Energy* **2016**, *1* (9), 16114.

(6) Shadike, Z.; Tan, S.; Lin, R.; Cao, X.; Hu, E.; Yang, X.-Q. Engineering and characterization of interphases for lithium metal anodes. *Chem. Sci.* **2022**, *13* (6), 1547-1568.

(7) Xu, Y.; Dong, K.; Jie, Y.; Adelhelm, P.; Chen, Y.; Xu, L.; Yu, P.; Kim, J.; Kochovski, Z.; Yu, Z.; et al. Promoting Mechanistic Understanding of Lithium Deposition and Solid-Electrolyte Interphase (SEI) Formation Using Advanced Characterization and Simulation Methods: Recent Progress, Limitations, and Future Perspectives. *Adv. Energy Mater.* **2022**, *12* (19), 2200398.

(8) Shadike, Z.; Lee, H.; Borodin, O.; Cao, X.; Fan, X.; Wang, X.; Lin, R.; Bak, S.-M.; Ghose, S.; Xu, K.; et al. Identification of LiH and nanocrystalline LiF in the solid–electrolyte interphase of lithium metal anodes. *Nat. Nanotechnol.* **2021**, *16* (5), 549-554.

(9) Tan, S.; Kim, J.-M.; Corrao, A.; Ghose, S.; Zhong, H.; Rui, N.; Wang, X.; Senanayake, S.; Polzin, B. J.; Khalifah, P.; et al. Unravelling the convoluted and dynamic interphasial mechanisms on Li metal anodes. *Nat. Nanotechnol.* **2023**, *18* (3), 243-249.

(10) Wagner-Henke, J.; Kuai, D.; Gerasimov, M.; Röder, F.; Balbuena, P. B.; Krewer, U. Knowledge-driven design of solid-electrolyte interphases on lithium metal via multiscale modelling. *Nat. Commun.* **2023**, *14* (1), 6823.

(11) Qian, J.; Henderson, W. A.; Xu, W.; Bhattacharya, P.; Engelhard, M.; Borodin, O.; Zhang, J.-G. High rate and stable cycling of lithium metal anode. *Nat. Commun.* **2015**, *6* (1), 6362.

(12) Ren, X.; Zou, L.; Cao, X.; Engelhard, M. H.; Liu, W.; Burton, S. D.; Lee, H.; Niu, C.; Matthews, B. E.; Zhu, Z.; et al. Enabling High-Voltage Lithium-Metal Batteries under Practical Conditions. *Joule* **2019**, *3* (7), 1662-1676.

(13) Cao, X.; Ren, X.; Zou, L.; Engelhard, M. H.; Huang, W.; Wang, H.; Matthews, B. E.; Lee, H.; Niu, C.; Arey, B. W.; et al. Monolithic solid–electrolyte interphases formed in fluorinated orthoformate-based electrolytes minimize Li depletion and pulverization. *Nat. Energy* **2019**, *4* (9), 796-805.

(14) Yu, Z.; Rudnicki, P. E.; Zhang, Z.; Huang, Z.; Celik, H.; Oyakhire, S. T.; Chen, Y.; Kong, X.; Kim, S. C.; Xiao, X.; et al. Rational solvent molecule tuning for high-performance lithium metal battery electrolytes. *Nat. Energy* **2022**, *7* (1), 94-106.

(15) Qiao, R.; Chuang, Y.-D.; Yan, S.; Yang, W. Soft X-Ray Irradiation Effects of Li2O2, Li2CO3 and Li2O Revealed by Absorption Spectroscopy. *PLOS ONE* **2012**, *7* (11), e49182.

(16) Vogt, L. I.; Cotelesage, J. J. H.; Dolgova, N. V.; Boyes, C.; Qureshi, M.; Sokaras, D.; Sharifi, S.; George, S. J.; Pickering, I. J.; George, G. N. Sulfur X-ray Absorption and Emission Spectroscopy of Organic Sulfones. *J. Phys. Chem. A* **2023**, *127* (16), 3692-3704.

(17) Yao, N.; Chen, X.; Shen, X.; Zhang, R.; Fu, Z.-H.; Ma, X.-X.; Zhang, X.-Q.; Li, B.-Q.; Zhang, Q. An Atomic Insight into the Chemical Origin and Variation of the Dielectric Constant in Liquid Electrolytes. *Angew. Chem. Int. Ed.* **2021**, *60* (39), 21473-21478.

(18) Kuai, D.; Balbuena, P. B. Inorganic Solid Electrolyte Interphase Engineering Rationales Inspired by Hexafluorophosphate Decomposition Mechanisms. *J. Phys. Chem. C* **2023**, *127* (4), 1744-1751.

(19) Liang, H.; Wang, L.; Song, Y.; Ren, D.; Wang, A.; Yang, Y.; Xu, H.; Sun, Y.; He, X. Manipulating Ion Transfer and Interface Stability by A Bulk Interphase Framework for Stable Lithium Metal Batteries. *Adv. Funct. Mater.* **2023**, *33* (37), 2303077.

(20) Camacho-Forero, L. E.; Smith, T. W.; Balbuena, P. B. Effects of High and Low Salt Concentration in Electrolytes at Lithium–Metal Anode Surfaces. *J. Phys. Chem. C* **2017**, *121* (1), 182-194.

(21) Henkelman, G.; Arnaldsson, A.; Jónsson, H. A fast and robust algorithm for Bader decomposition of charge density. *Comput. Mater. Sci.* **2006**, *36* (3), 354-360.

(22) Tang, W.; Sanville, E.; Henkelman, G. A grid-based Bader analysis algorithm without lattice bias. *J. Phys. Condens. Matter* **2009**, *21* (8), 084204.

(23) Hu, Y.-Y.; Liu, Z.; Nam, K.-W.; Borkiewicz, O. J.; Cheng, J.; Hua, X.; Dunstan, M. T.; Yu, X.; Wiaderek, K. M.; Du, L.-S.; et al. Origin of additional capacities in metal oxide lithium-ion battery electrodes. *Nat. Mater.* **2013**, *12* (12), 1130-1136.

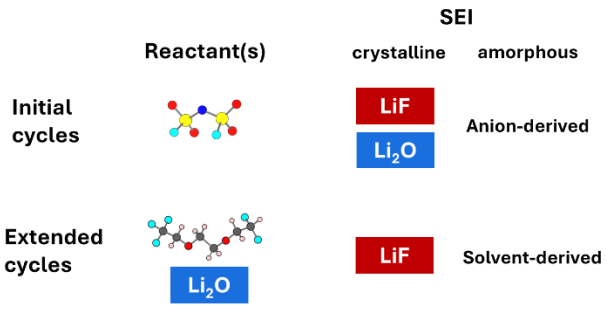
SEI
Reactant(s)
crystalline
amorphous
Initial cycles
LiF
Li2O
Anion-derived
Extended cycles
Li2O
LiF
Solvent-derived